Strojniški vestnik - Journal of Mechanical Engineering 66(2020)9, 494-504

DOI:10.5545/sv-jme.2020.6688
Original Scientific Paper
Received for review: 2020-03-24
Received revised form: 2020-05-19
Accepted for publication: 2020-07-15

# Microstructure and Property Modification of Cold Sprayed Coatings Using Different Grain Sizes of $Cr_3C_2$-25(Ni20Cr) Composite Powder

Anna Trelka[1,*] – Wojciech Żórawski[2] – Anna Góral[1]

[1]Institute of Metallurgy and Materials Science, Polish Academy of Sciences, Poland
[2]Laser Processing Research Centre, Kielce University of Technology, Poland

*This article describes the microstructure and mechanical properties of $Cr_3C_2$-25(Ni20Cr) cermet coatings cold-sprayed on Al 7075 alloy substrates. The study aimed to determine the effect of three different powder grain sizes and three different standoff distances on the microstructure (phase composition, surface topography, volume fraction and distribution of the $Cr_3C_2$ phase in the Ni20Cr matrix and porosity) and the mechanical properties (hardness and abrasive wear resistance) of the $Cr_3C_2$-25(Ni20Cr) coatings. The examinations revealed that the thickness of the coatings obtained with the same duration and feed rate decreased with increasing powder grain size and standoff distance. The coatings produced from powders with smaller particles had higher hardness and more compact structures than the coatings obtained from powders where the particles were larger (more than 40 μm). The coatings produced from finer powders were also more resistant to abrasive wear.*

**Keywords: $Cr_3C_2$-25(Ni20Cr) composite coating; cold spraying; microstructure; powder grain size; standoff distance; mechanical properties**

**Highlights**

- *The grain size and standoff distance significantly affect the microstructure and properties of $Cr_3C_2$-25(Ni20Cr) coatings, e.g., the content of the ceramic phase increases by over 40 % as the grain size increases.*
- *$Cr_3C_2$-25(Ni20Cr) cold-sprayed coatings revealed a compact and uniform microstructure.*
- *The thickness of the cold sprayed $Cr_3C_2$-25(Ni20Cr) coatings (obtained with the same duration and feed rate) decreased with increasing particle size of the powder and increasing standoff distance.*
- *The coatings made from the powder with the grain size of 9.5 μm to 55.3 μm had the highest hardness, while those made from the powder with the grain size of 40 μm to 55.3 μm the lowest.*

## 0 INTRODUCTION

Thermally sprayed composite coatings are common in industrial applications because of the wide variety of materials from which they can be made as well as numerous methods by which they can be deposited. In recent years, there has been a demand for innovative coatings to improve the properties of coated materials, which has led to a high development of research in the field of composite deposits **[1]** and **[2]**. Coatings are designed mainly to improve the durability and environmental resistance of machine parts; they may also impart catalytic properties to them. Surface layers serve to enhance the mechanical properties of the underlying material, protecting it against deterioration due to corrosion, friction, abrasive wear, unfavourable temperatures and aggressive environments **[3]** to **[5]**. $Cr_3C_2$-NiCr coatings have been widely discussed in the literature because of their excellent resistance to abrasive wear **[6]** to **[12]**. Composite coatings are used in environments in which severe erosion and corrosion occur **[13]** to **[15]**. $Cr_3C_2$-25(Ni20Cr) coatings are often produced using thermal spraying methods, especially high-velocity oxygen fuel **[7]**, **[8]**, **[10]** and plasma spraying **[11]**, but, recently, also by cold spraying **[6]**, **[9]** and **[12]**. In some applications, cold spraying is superior to the other thermal spraying methods **[16]** because the gas temperature is lower than the melting point of the feedstock material, the powder particles do not undergo severe oxidation, and there is no phase change or growth of particles. In other words, problems typical of thermal spraying do not occur. The low porosity of cold-sprayed coatings and the absence of oxides in them may result in very high electrical conductivity as well as good corrosion resistance **[17]** and **[18]**. Such coatings are formed as a consequence of severe plastic deformation of powder particles, adiabatic shear instability and mechanical interlocking **[19]**. Powder particles are in the solid-state when they reach the substrate surface. Particles carried by the first stream remove all impurities together with the outer layer of oxides, which activates the substrate, making the next layers of particles adhere easily to it **[20]**. A vital cold spray parameter is critical velocity, dependent on the type, morphology and size of the feedstock particles **[21]** and **[22]**. As


*Corr. Author's Address: Institute of Metallurgy and Materials Science, Polish Academy of Sciences, ul. Reymonta 25, 30-059 Krakow, Poland, a.trelka@imim.pl

pointed out by Sevillano et al. [23], the presence of small ceramic particles uniformly distributed in the metallic matrix of $Al_2O_3$-Ni composite coatings is beneficial, because the ceramic phase can act as a barrier against the propagation of cracks, while the metallic particles harden and strengthen under the impact of the subsequent layers, which may result in higher hardness and rigidity of the coatings. Celotto et al. [24] write that to deposit coatings successfully, various metallic particles 5 μm to 50 μm in size should be used. Powders with metallic particles smaller than 5 μm have poor flowability, and the reason is their lower weight and therefore insufficient kinetic energy to deform and adhere to the substrate. Particles larger than 50 μm have too much inertia and as such cannot be accelerated to a velocity higher than the critical velocity [24]. Sova et al. [15], who analyse cold sprayed $Al_2O_3$-Al, SiC-Al, $Al_2O_3$-Cu and SiC-Cu composite coatings with different sizes of ceramic phase particles (19 μm to 25 μm and 135 μm to 141 μm), indicate that, regardless of the type of material used, smaller particles ensured higher deposition efficiency of the feedstock and higher thickness of the coatings. Composite powders with larger particles contributed to coating erosion during deposition, and consequently lower efficiency of the deposition process. Another parameter that significantly affects the efficiency of the cold-spraying process and the quality of the coatings is the standoff distance between the nozzle and the substrate. As recommended in [25], the standoff distance should be less than or equal to the length of the non-scattered portion of the initial jet.

The current challenge facing researchers is to develop new cold sprayed composite coatings with properties desirable in the automotive and aviation industries. Although some research has been carried out on cold sprayed composite coatings [5], [6], [9], [12] to [15], [23] and [26] to [29], no studies analysing the combined effect of the standoff distance and the powder grain size have been found. This study was undertaken to address the knowledge gap by investigating how the two parameters influenced the microstructure and the mechanical properties of the $Cr_3C_2$-25(Ni20Cr) coatings.

## 1 MATERIALS AND METHODS

The cermet coatings were deposited on Al 7075 alloy substrates using $Cr_3C_2$-25(Ni20Cr) Diamalloy 3004 powder (Oerlikon Metco Europe GmbH, the Polish Division, Poznań, Poland) composed of balance Cr, 18.75 % Ni, 9.75 % C, 2.25 % other (max). The cold-spraying process was performed with an Impact Innovations 5/8 Cold Spray System, (Impact Innovations GmbH, Rattenkirchen, Germany) mounted on a Fanuc M-20iA robot arm (ZAP Robotyka, Ostrów Wielkopolski, Poland). Table 1 shows the cold spray process parameters.

Table 1. *Parameters of the cold sprayed $Cr_3C_2$-25(Ni20Cr) coatings*

| Parameter | | Value |
|---|---|---|
| Pressure [MPa] | | 4 |
| Temperature [°C] | | 800 |
| Standoff distance [mm] | | 10; 30; 50 |
| Process gas | | $N_2$ |
| Powder grain size [$\mu$m] | | (DL: 9.5 to 40); |
| | | (DO: 9.5 to 55.3); |
| | | (DT: 40 to 55.3) |
| Powder feeder rate [g/min] | | 95 ± 5 |
| Number of layers | | 40 |
| Speed of robot arm [m/s] | | 0.3 |
| Nozzle | type | convergent-divergent |
| | length [mm] | 161 |
| | designation | INJECTOR–OUT 1-SIC (10202.00.0.01) |

The experiments were carried out for three different powder grain sizes and three different nozzle-substrate standoff distances: 10 mm, 30 mm, and 50 mm. The original commercially available $Cr_3C_2$-25(Ni20Cr) powder, denoted by DO, had a grain size ranging from 9.5 μm to 55.3 μm (Fig. 1), which was established using a Malvern Mastersizer analyser (HELOS Particle Size Analysis, Sympatec GmbH System-Partikel-Technik, Clausthal-Zellerfeld, Germany). The other powders, DL and DT, were obtained by dry sieving the DO powder through a 40 μm mesh screen. The DL powder had a grain size in the range of 9.5 μm to 40 μm, while the DT powder was composed of particles in the range of 40 μm to 55.3 μm. The content of the ceramic phase in the powders determined using X-ray diffraction and image analysis (ImageJ) based on the powder cross-section microstructures (10 images in the case of each powder) obtained using SEM was: DL (77.6 ± 3.9 % vol.), DO (78.4 ± 2.7 % vol.), DT (80.3 ± 3.1 % vol.). Nine samples were analysed: DL1, DL3, DL5, DO1, DO3, DO5, DT1, DT3 and DT5. The symbols correspond to the powder grain size and the standoff distance. For example, DL1, DL3 and DL5 represent coatings produced from the DL powder at standoff distances of 10 mm, 30 mm and 50 mm, respectively.

The coating thickness analysis was carried out for the optical microscope images using ImageJ software. Prior to the microscopic examinations, the specimens were cut, mounted in synthetic resin, ground with

400 to 7000 grit paper, polished to 3 μm, 1 μm and 0.25 μm diamond suspension finishes using a Presi MecaPol P320 (PRESI France, Eybens, France) setup, washed and dried.

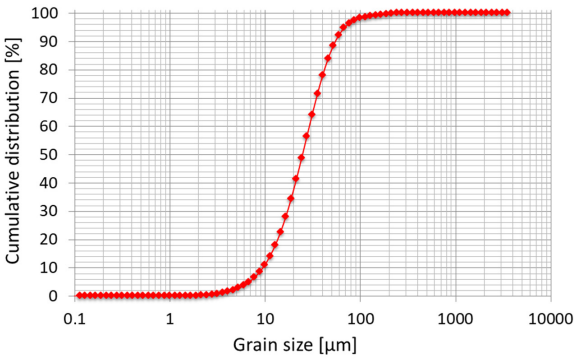


**Fig. 1.** *Grain size distribution for the $Cr_3C_2$-25(Ni20Cr) (DO) powder*

The cross-sectional observations with a Leica DM IRM optical microscope (Leica Microsystems Wetzlar GmbH, Wetzlar, Germany) aimed to determine the thickness of the coatings and visually inspect their quality. The microstructure of the cold sprayed $Cr_3C_2$-25(Ni20Cr) coatings was characterised by scanning electron microscopy (FEI /Philips XL30, FEI Company, Oregon, United States). A Bruker D8 Discover diffractometer (Bruker AXS GmbH, Karlsruhe, Germany) with CoKα radiation (a wavelength of 1.7903 Å) was used to study the phase compositions of the powders and the coatings. The volume fraction of the ceramic phase and the porosity in the coatings were measured using the ImageJ software. The surface topography analysis was performed with a Keyence VHX-7000 microscope (Keyence Corporation, Osaka, Japan). Three surfaces were selected and characterised on the basis of the respective 600 μm × 3000 μm topographical maps with five roughness parameters each. A CSM Instruments (Anton Paar GmbH, Graz, Austria) low-load Vickers hardness tester (HV0.3) was used to determine the coating hardness in the cross-section. In each case, the hardness result was an average of 12 measurements taken at different points. The coating hardness was measured in accordance with the standard ISO 6507-1:2018(en) [30]. Hardness was measured according to the diagonal of the imprint. The abrasive wear tests were carried out using an ITEE T-07 tester (The Institute for Sustainable Technologies, Radom, Poland) (dry sand-rubber wheel) and loose abrasive $Al_2O_3$ particles 250 μm to 300 μm in size, at a flow rate of 250 g/min, a wheel (Ø50 × 20) rotation speed of 200 rpm, and a load of 50 N.

## 2 RESULTS

### 2.1 Characterisation of the $Cr_3C_2$-25(Ni20Cr) powders

Fig. 2 shows the morphologies of the $Cr_3C_2$-25(Ni20Cr) Diamalloy 3004 powders differing in the grain size (DL, DO and DT). All the powders consist of a metallic phase and a ceramic phase. The particles of the former are almost spherical or elongate in shape, while those of the latter are irregularly shaped with sharp and uneven edges. As can be seen from Figs. 2a and c, there is a significant difference in grain size between the DL powder (less than 40 μm) and the DT powder (more than 40 μm). Fig. 3 shows the phase analysis for the $Cr_3C_2$-25(Ni20Cr) powders. From the diffractogram, it is evident that there are two phases: the $Cr_3C_2$ ceramic phase (cell parameters: a = 5.533 Å, b = 2.829 Å and c = 11.472 Å) and the metallic $Cr_{0.25}Ni_{0.75}$ phase (cell parameter: a = 3.552 Å). The $Cr_{0.25}Ni_{0.75}$ phase contains 22.8 wt% Cr and 77.2 wt% Ni, according to the PDF 04-003-7001 card.

### 2.2 Characterisation of the $Cr_3C_2$-25(Ni20Cr) coatings

#### *2.2.1 Thickness, Morphology and Microstructure*

The thickness measurement results obtained for the DL, DO, and DT coatings are compared in Fig. 4. The data indicate that the coating thickness decreases with

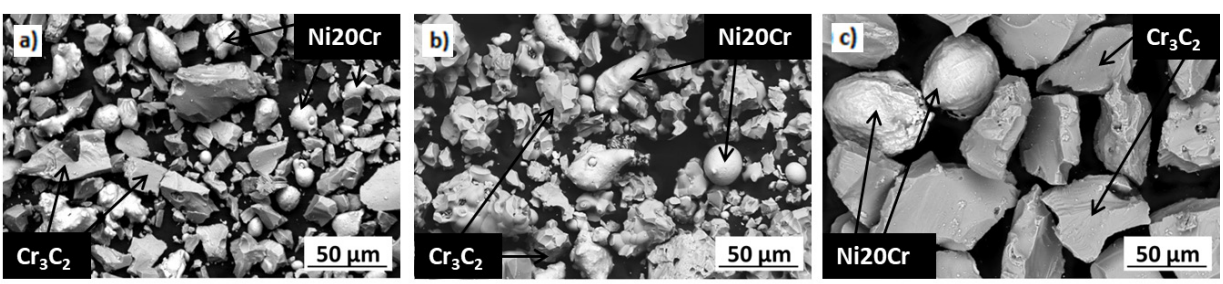


**Fig. 2.** *SEM-BSE (backscattered electrons) images depicting the morphologies of the $Cr_3C_2$-25(Ni20Cr) powders a) DL b) DO c) DT*

increasing standoff distance. From Fig. 4, it is also clear that the greater the powder grain size, the thinner the coating.

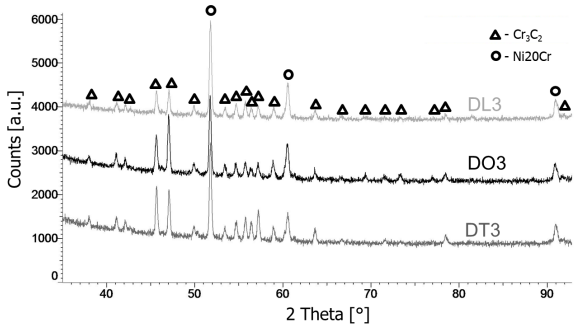


**Fig. 3.** *X-ray diffraction patterns for the DL3, DO3 and DT3 powders*

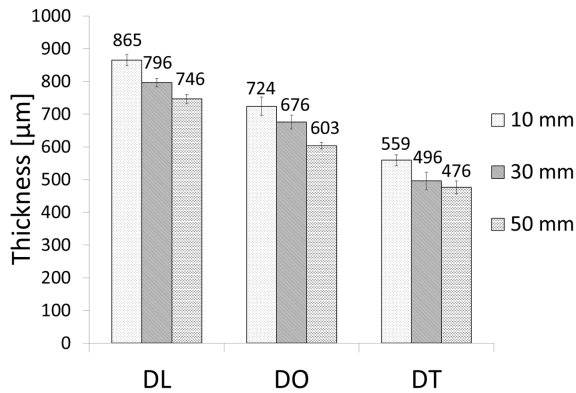


**Fig. 4.** *Effect of the grain size and standoff distance on the thicknesses of the $Cr_3C_2$-25(Ni20Cr) coatings: DL (9.5 µm to 40 µm), DO (9.5 µm to 55.3 µm), DT (40 µm to 55.3 µm)*

Fig. 5 shows the phase compositions of the DL3, DO3, and DT3 coatings. The microstructural analysis of the coatings revealed that they also consisted of a ceramic phase (chromium carbide ($Cr_3C_2$)) and a metallic phase ($Ni_{0.75}Cr_{0.25}$).

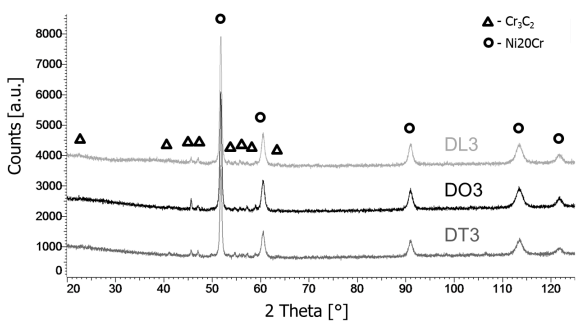


**Fig. 5.** *X-ray diffraction patterns for the DL3, DO3 and DT3 coatings*

A significant advantage of the cold-spray process, confirmed through the X-ray diffraction analysis, is that no change in the phase composition occurs during deposition. Cold-spraying does not cause oxidation of the material or formation of new phases, as is the case with other thermal spraying methods.

The surface morphologies of the coatings tested are shown in Fig. 6. The arrows indicate the ceramic phase. The analysis of the DL coatings revealed the presence of the Ni20Cr phase with embedded ceramic phase $Cr_3C_2$ particles. Visual observation revealed that the area of the metallic phase was the smallest when the standoff distance was 10 mm (Fig. 6a). In the coatings produced at 30 mm (DL3) or 50 mm (DL5), the area of the metallic phase was more extensive, while the ceramic phase was highly fragmented (Figs. 6b and c, respectively). The examination of the DO coatings made from the original powder shows that the largest zone of the metallic phase was obtained for DO3, sprayed at a distance of 30 mm (Fig. 6e) and that it was a result of high plastic deformation. As can be seen from the morphologies of the coatings presented in Fig. 6, the highest volume fraction of the $Cr_3C_2$ ceramic phase at the surface is observed for DT deposits. During the deposition process, the brittle ceramic particles were crushed and unevenly distributed in the metallic phase, giving the impression that powder with smaller particles was used. The higher amount of ceramic particles at the surface was responsible for the higher roughness of the DT coatings.

The surface topography parameters of the coatings deposited at the same standoff distance of 30 mm but differing in initial powder grain size are presented in Fig. 7 and Table 2. The surface roughness parameter, i.e., the arithmetic mean height ($S_a$), increased with increasing powder grain size. The difference in roughness between the DL3 and DO3 coatings (Figs. 7a and b, respectively) was small, with the difference in maximum height ($S_z$) being 10.1 µm. In the case of the DT3 coating (Fig. 7c), the parameter was more than twice as high as those obtained for DL3 or DO3. All the parameters indicate that the grain size is the factor affecting the surface topography. The texture aspect ratio of the surface ($S_{tr}$) decreased with increasing powder grain size. The arithmetic mean peak curvature ($S_{pc}$) represents the arithmetic mean of the principal curvature of the peaks on the surface. The lower its value, the more rounded the shapes of the points of contact. The developed interfacial area ratio ($S_{dr}$) is expressed as the percentage of the definition area's additional surface area contributed by the texture as compared to the planar definition area.

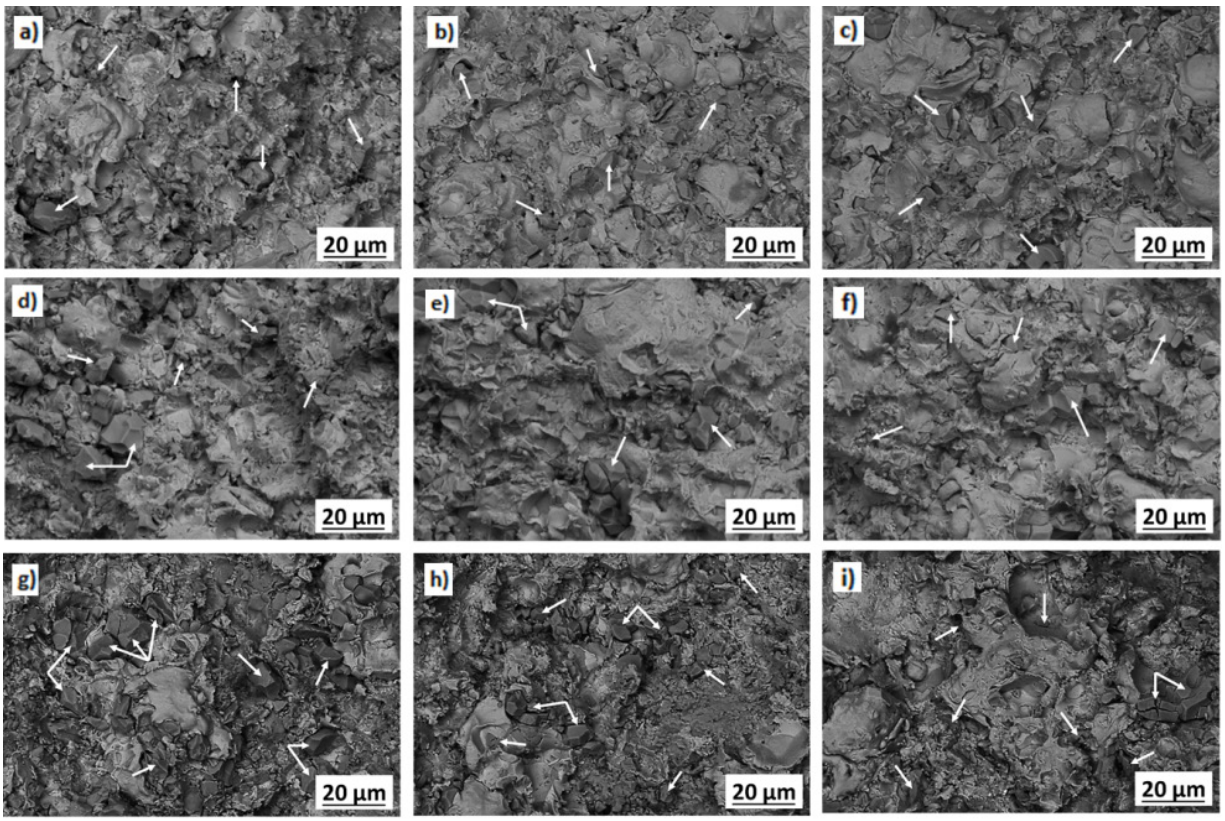


**Fig. 6.** *SEM-BSE images showing the surface morphologies of the $Cr_3C_2$-25(Ni20Cr) coatings from powders differing in grain size cold sprayed at three different standoff distances: a) DL1, b) DL3, c) DL5, d) DO1, e) DO3, f) DO5, g) DT1, h) DT3 i) DT5; arrows indicating $Cr_3C_2$*

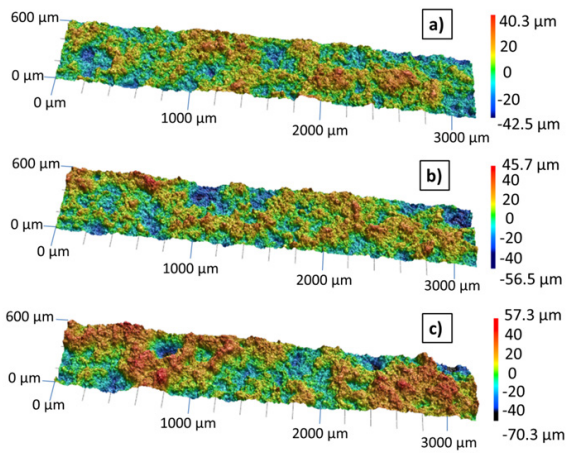


**Fig. 7.** *Surface topographies of the $Cr_3C_2$-25(Ni20Cr) coatings from powders differing in grain size produced at a standoff distance of 30 mm a) DL3, b) DO3, c) DT3*

The parameters $S_{pc}$ and $S_{dr}$ increase with increasing grain size (Table 2).

Fig. 8 shows cross-sectional views of the different cold sprayed coatings. The deposits are composed of the ceramic $Cr_3C_2$ phase, marked in dark grey, and the metallic Ni20Cr phase, visible as light grey. The substrate is black. The DL coatings have small ceramic phase particles evenly distributed in the Ni20Cr alloy matrix, which is particularly visible for the DL3 coating. The $Cr_3C_2$ phase in the DL3 and DL5 coatings is in the form of strands. The most uniform microstructure is that of the DL3 coating. The microstructures of the DO coatings seem more compact than those of the DL and DT coatings. The ceramic particles are distributed in the metallic matrix in the form of strands. The analysis of

**Table 2.** *Area surface topography parameters determined for the $Cr_3C_2$-25(Ni20Cr) coatings*

| Coating surface | Parameters* | | | | |
|---|---|---|---|---|---|
| | Height | | Spatial | Feature | Hybrid |
| | $S_a$ [µm] | $S_z$ [µm] | $S_{tr}$ | $S_{pc}$ [1/mm] | $S_{dr}$ |
| DL3 | 5.1 | 55.8 | 1.0 | 958.5 | 0.5 |
| DO3 | 5.7 | 65.9 | 0.9 | 999.3 | 0.6 |
| DT3 | 6.7 | 138.4 | 0.7 | 1143.8 | 0.9 |

* $S_a$ arithmetic mean height, $S_z$ maximum height, $S_{tr}$ texture aspect ratio, $S_{pc}$ arithmetic mean peak curvature, $S_{dr}$ developed interfacial area ratio

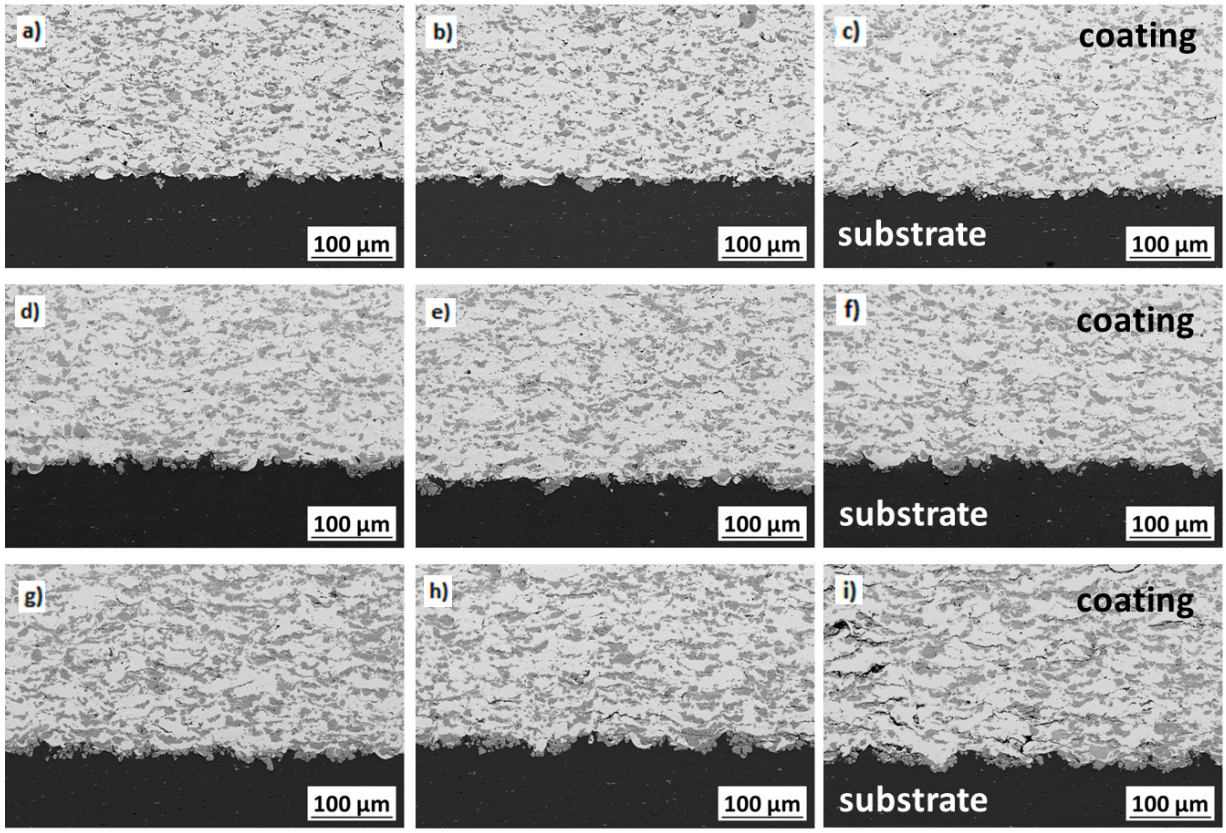


**Fig. 8.** *SEM-BSE images depicting the cross-sectional microstructures of the $Cr_3C_2$-25(Ni20Cr) coatings from powders differing in grain size cold sprayed at three different standoff distances: a) DL1, b) DL3, c) DL5, d) DO1, e) DO3, f) DO5, g) DT1, h) DT3, i) DT5*

the average porosity of all the coatings (DL, DO and DT) shows that the DO coatings exhibit the lowest porosity, ranging from 1.7 ± 0.4 % vol. to 1.9 ± 0.4 % vol. (Fig. 9). When single coatings are considered, the DL3 coating has the lowest porosity (1.6 % vol.). The volume fraction of the ceramic phase in the DT coatings, varying from 38.8 ± 2.8 % vol. to 39.7 ± 0.9 % vol., is much higher than those in the DL, being in the range of 26.4 ± 0.8 % vol. to 28.8 ± 1.9 % vol. or DO, ranging between 31.8 ± 1.8 % vol. and 33.8 ± 1.6 % vol. However, high fragmentation of ceramic particles is visible in the region closest to the substrate. In the case of the DT5 coating, the fragmentation affected porosity, which was about 1 % vol. higher than in the other coatings. The microstructures of the coatings are less compact, which is associated with the cracking and fragmentation of the ceramic phase particles (Figs. 10b and c). The porosity observed between the crushed $Cr_3C_2$ particles could have been the result of particle crumbling during sample preparation for scanning electron microscopy (Fig. 10).

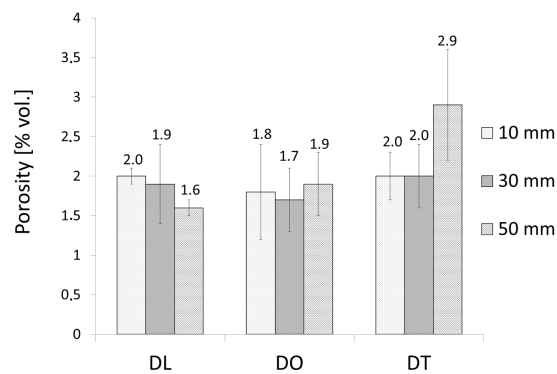


**Fig. 9.** *Porosities (% vol.) of the $Cr_3C_2$-25(Ni20Cr) coatings*

The results provided in Fig. 11 indicate that the volume fraction of the ceramic phase decreased with increasing standoff distance; this, however, is not true for the DO5 coating. Higher volume fractions of the ceramic phase were observed when the feedstock powder particles were larger. The highest volume fraction of the ceramic phase was reported for the DT coatings produced from the powder with particles greater than 40 µm, while the lowest for the DL

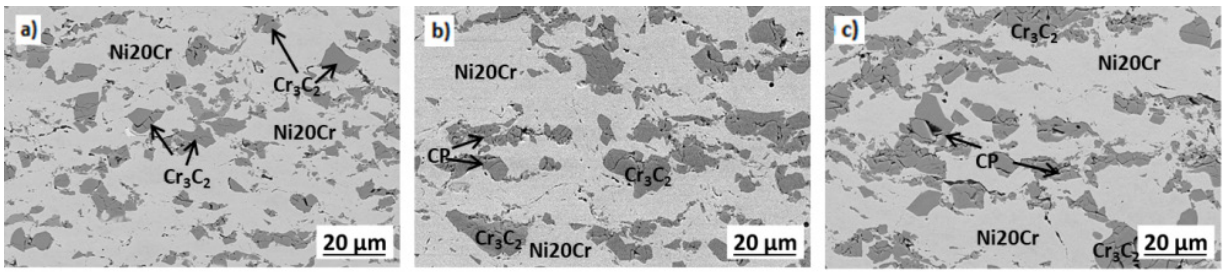


**Fig. 10.** *SEM-BSE cross-sectional views of the coating microstructures: a) DL3, b) DO3, c) DT3; CP - porosity caused by the crumbling of finer ceramic particles*

coatings. The difference between them was 10 % vol., which may have resulted from the bouncing of small ceramic particles off the surface during the cold spray process. The effect of the standoff distance on the volume fraction of the ceramic phase in the coatings was negligible (about 2 % vol.). Fig. 9 shows that the highest porosity occurred at a standoff distance of 50 mm when powder with a grain size greater than 40 µm was used.

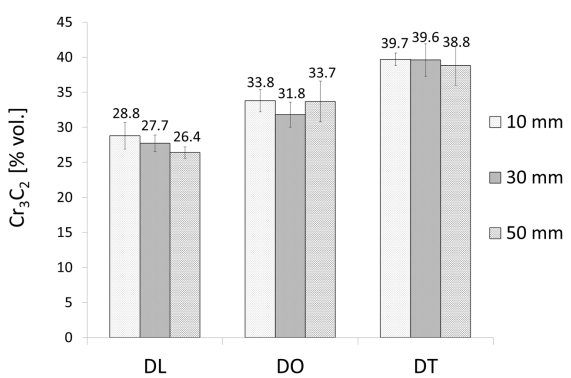


**Fig. 11.** *$Cr_3C_2$ particles embedded in the $Cr_3C_2$-25(Ni20Cr) coatings (% vol.)*

### 2.2.2 Mechanical and Tribological Properties

The hardness measurement results show that the DO coatings, obtained from the original powder, have the highest hardness, while the DT coatings the lowest (Fig. 12). The hardness of the DL coatings was slightly lower than that of the DO coatings. The low hardness of the DT coatings was a consequence of their high microstructural porosity related to the crumbling of the high amount of ceramic phase embedded in the Ni20Cr matrix. The high values of the standard deviation obtained for the DT specimens indicate a non-uniform structure resulting from the high porosity of the coatings. No significant relationship was observed between the coating hardness and the standoff distance. The difference between the highest and lowest values of hardness obtained for each standoff distance was the same, irrespective of the grain size; it was about 20 HV0.3. Fig. 13 shows the load-displacement curves and the hardness indentations obtained for the DO3 and DT3 specimens.

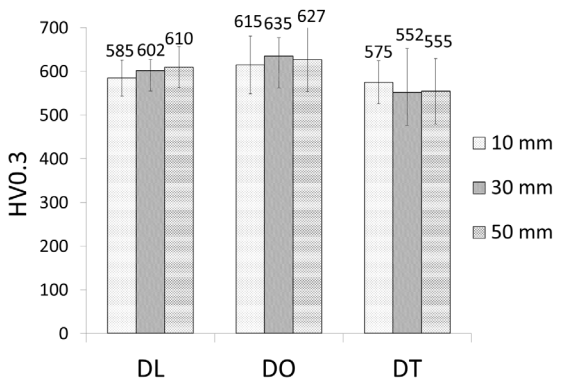


**Fig. 12.** *Hardness of the $Cr_3C_2$-25(Ni20Cr) coatings*

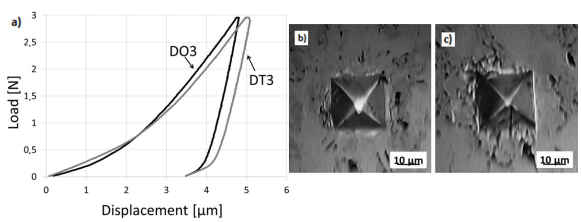


**Fig. 13.** *a) A load-displacement curve and b) hardness indentations for the DO3 and c) DT3 $Cr_3C_2$-25(Ni20Cr) coatings*

The indentation in the DO3 coating was smaller than that in the DT3 (Figs. 13b and c, respectively), which suggests its higher hardness. The porosity observed around the irregularly shaped indentation in the DT3 specimen (Fig. 13c) had a considerable effect on the coating hardness. From the load-displacement curves in Fig. 13a, it is also clear that the hardness of

the DT3 coating is lower. At a load of 2.942 N, the indenter displacement was higher than 4.5 μm for the DO3 specimen, while for DT3 it was higher than 5 μm.

Fig. 14 shows the mass loss for the DL3, DO3 and DT3 coatings after the abrasive wear tests. The DL3 coating containing the lowest volume fraction of the ceramic phase in comparison with the DO3 and DT3 deposits revealed the most considerable mass loss. The DO3 and DT3 coatings had an identical mass loss after 30 min of the abrasive wear tests (125 mg), which was 29 % lower than that reported for DL3 (161 mg). It was also found that the wear time for DT3 was shorter (30 min) than for the other coatings (40 min). Compared to DL3 or DO3, this coating was about 37.7 % thinner, which was the reason for its shorter wear time. The microstructures of the DL3 and DO3 coatings studied after the abrasive wear tests by optical and scanning electron microscopes are shown in Fig. 15. The differences in the appearance of wear track between the coatings after the tests with loose abrasive corundum ($Al_2O_3$) were insignificant. The wear track reported for DO3 (Fig. 15b) was more uneven than that observed in DL3 (Fig. 15a), which was probably due to the greater grain size and the higher content of ceramic particles, which broke off during friction.

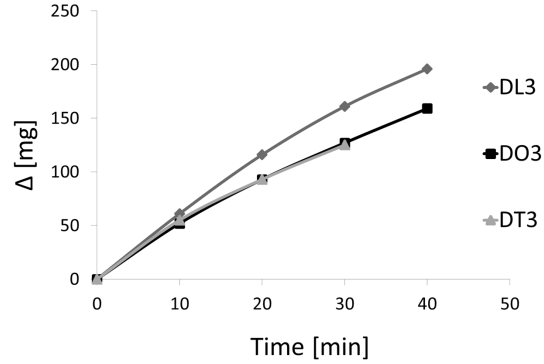


**Fig. 14.** *Mass loss during the abrasive wear test*

## 3 DISCUSSION

This study provides new insights into cold-sprayed composite coatings, especially the effects of the powder grain size and the standoff distance on the microstructure and properties of the $Cr_3C_2$-25(Ni20Cr) cermet coatings.

The comparison of the diffraction patterns of the feedstock powders with those of the cold sprayed coatings revealed several differences. The relative intensity of the chromium carbide peaks was higher for the powders than for the coatings (Figs. 3 and

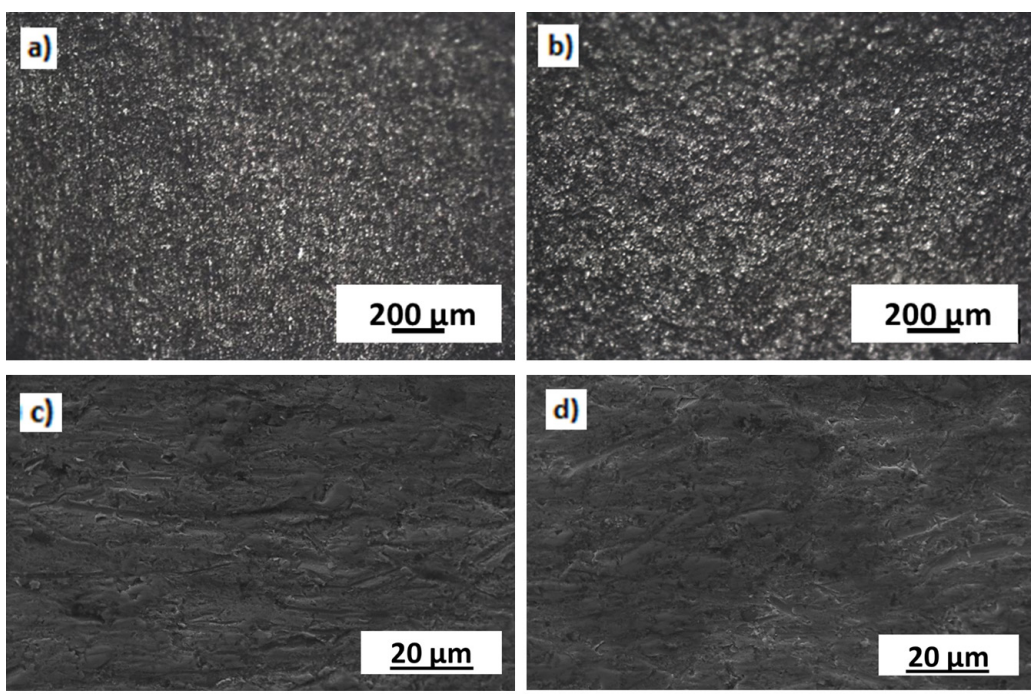


**Fig. 15.** *Microstructures of the $Cr_3C_2$-25(Ni20Cr) coatings after the abrasive wear tests: a) and c) DL3, b) and d) DO3 performed using optical (a, b; magnification 100x) and scanning electron microscope (c, d; magnification 2000x)*

5, respectively). This suggests that the content of chromium carbide decreased during the deposition process, which is confirmed by the results in Fig. 11. Much fewer $Cr_3C_2$ particles were found in the coating structure, and this was because they did not deform plastically during the cold spraying process; instead, they bounced off the substrate surface. The broader diffraction peaks for the chromium-nickel phase indicate a decrease in the grain size. Similar relationships are reported by Wolfe and Eden **[12]** for $Cr_3C_2$-NiCr.

The microstructural analysis of the $Cr_3C_2$-25(Ni20Cr) coatings in cross-section (Fig. 8) reveals that the ceramic particles in the DL coatings are smaller and distributed evenly, while those in the DT coatings are larger and arranged in the strands-like elongated forms. Small ceramic particles uniformly embedded in a coating are considered beneficial because they can act as a barrier against crack propagation. They also play important roles of peening and roughing of the layers during deposition, modifying the coating growth and, as a consequence, the coating properties **[29]**. Metallic particles, in contrast, harden and strengthen under the impact of the subsequent layers, which may cause higher hardness and rigidity of the coatings **[23]**. Ni20Cr particles are plastically deformed and bonded both with the substrate and each other as a result of mechanical interlocking and adiabatic shear instability. The significant loss of the ceramic phase in relation to the metallic phase is explained by Fernandez and Jodoin **[9]**, who argue that, when ceramic particles crack upon impact, some are lost as a result of weak bonding between them and are blown away by the gas stream. They also report an increase in the volume fraction of the NiCr phase. The coating thickness is strictly related to the deposition efficiency of the process **[31]**. Sova et al. **[15]** state that, for coatings made from $Al_2O_3$-Al, SiC-Al, $Al_2O_3$-Cu and SiC-Cu powders, the deposition efficiency strongly depends on the size of powder grains and is higher for smaller particles. This study confirmed this relationship, i.e., that the thickness of the $Cr_3C_2$-25(Ni20Cr) coatings decreased with increasing powder grain size. The DL coatings, which were made from the smallest particles, were the thickest. Large ceramic particles phase are brittle, which hinders the bonding of the sprayed material with the previously deposited layer **[9]**. The analysis shows that regardless of the size of the powder grains, an increase in the standoff distance causes a decrease in the thickness of the coatings (Fig. 4) and a slight decrease in the volume fraction of the $Cr_3C_2$ ceramic phase, the exception being the DO5 coating sprayed at a distance of 50 mm (Fig. 11). The difference in thickness between the coatings obtained at the spraying distance of 10 mm and those produced at 50 mm was about 100 μm, no matter how large the powder particles were (DL, DO or DT). In cold spraying, longer standoff distances result in thinner coatings because of the bouncing of particles off the surface during the formation of subsequent coating layers, which may be due to an increase in the particle momentum, being a result of a longer standoff distance. Smaller particles achieve higher velocities than larger ones, and since powders are a mixture of particles of different sizes, some of the powder is deposited, while the remainder bounces off **[16]**.

The greater size of grains in the DT3 coatings resulted in a surface roughness of at least 18 % higher than for the other coatings. Higher roughness can affect coatings both positively and negatively. While the subsequent layers deposited on the substrate bond easily, the significant fragmentation of ceramic particles increases the undesirable porosity **[9]**. The high value of the roughness parameter $S_a$ observed for the DT3 coating was due to the higher volume fraction of ceramic particles. The microstructural examination showed that porosity occurred mainly where the particles of the ceramic phase crumbled (Fig. 10c). The preparation of the specimen cross-sections for the SEM examinations also increased the porosity of the composite materials. During that process, very small fragments of the ceramic particles broke off and fell out. All the coatings studied were characterised by low porosity (less than 3 % vol.). Sevillano et al. **[23]** observed a similar relationship for Ni-$Al_2O_3$ coatings, which had low porosity (about 3 % vol.) with pores found mainly in cracks in the ceramic phase.

As for the mechanical properties, the DO coatings exhibited the highest hardness, ranging between 615 ± 66 and 635 ± 42 HV0.3, while the DT ones had the lowest, varying from 552 ± 100 to 575 ± 49 HV0.3 (Fig. 12). According to the literature **[26]**, the higher volume fraction of the ceramic phase, the higher hardness of the Ni-WC composite coatings. No such observations were made in this study. The reason for that was the cracking of large $Cr_3C_2$ particles during the spraying process, which resulted in lower hardness of the coatings. In the $Cr_3C_2$-25(Ni20Cr) coatings produced from the DO and DL powders, lower volume fractions of the ceramic phase did not lead to lower hardness because the microstructures of the coatings were compact (Fig. 8). They showed a small difference in hardness of about 4.5 % (Fig. 12). The coatings made from the finest powder showed higher mass loss during the abrasive wear tests (Fig. 14).

This was attributed to the lower volume fraction and smaller size of the ceramic phase particles (Fig. 11).

From the results concerning the coating thickness, hardness, abrasion resistance, porosity and content of ceramic phase, it can be concluded that the $Cr_3C_2$-25(Ni20Cr) coatings produced from the original powder (DO) sprayed at a distance of 30 mm have the best properties. They are compact and reveal the high hardness (635 ± 42 HV0.3), a high volume fraction of the ceramic phase (31.8 ± 1.8 % vol.), low porosity (1.7 ± 0.4 % vol.), and considerable thickness (676 ± 21 μm), which confirms good relative deposition efficiency. The coatings made from smaller (9.5 μm to 40 μm) powder grains at different standoff distances (DL1, DL3, DL5) had higher thickness, but they showed lower hardness. The DT3 coating, in contrast, had a high content of the ceramic phase but low hardness and highest porosity; it was also the thinnest of all the deposits. The experimental data indicate that the desired mechanical properties of $Cr_3C_2$-25(Ni20Cr) coatings can be achieved economically by selecting the optimal parameters, i.e., powder grain size ranging from 9.5 μm to 55.3 μm and a standoff distance of 30 mm.

## 4 CONCLUSIONS

The purpose of this study was to determine how the size of the $Cr_3C_2$-25(Ni20Cr) powder particles and the nozzle-substrate standoff distance (10 mm, 30 mm or 50 mm) affect the microstructure and mechanical properties of the $Cr_3C_2$-25(Ni20Cr) cermet coatings cold sprayed on the Al 7075 substrate. The following conclusions have been drawn from the study results:

1. All the $Cr_3C_2$-25(Ni20Cr) coatings had a compact microstructure; however, those that were produced from the powder with the largest particles had higher porosity.
2. The cold-sprayed coatings obtained from the powder with particles greater than 40 μm (DT) had the highest volume fraction of the $Cr_3C_2$ ceramic phase. The volume fraction of the $Cr_3C_2$ ceramic phase was the lowest for the coatings produced from powder with particles smaller than 40 μm (DL). The standoff distance had little effect on the content of the ceramic phase in the coatings.
3. The thickness of the cold-sprayed $Cr_3C_2$-25(Ni20Cr) coatings decreased with increasing powder grain size and increasing standoff distance.
4. The coatings made from the powder with the original grain size (DO: 9.5 μm to 55.3 μm) had the highest hardness. The hardness of the DT coatings made of the powder with the grain size 40 μm to 55.3 μm, in contrast, was the lowest.
5. The cold-sprayed coatings obtained from the powders with larger particles (DO and DT) had higher resistance to abrasive wear when tested with loose abrasive particles than the coatings obtained from the finest powder.
6. The $Cr_3C_2$-25(Ni20Cr) coatings produced from the DO powder at a standoff distance of 30 mm had the best properties, i.e., high thickness, high hardness, high resistance to abrasive wear, a relatively high volume fraction of the $Cr_3C_2$ phase and low porosity.

## 5 ACKNOWLEDGEMENTS

This work was supported by the National Science Centre, Poland (Project No 2017/25/B/ST8/ 02228).

## 6 REFERENCES

[1] Yi, H., Liu, X., Che, J., Liang, G. (2020). Thermochemical compatibility between $La_2(Ce1\text{-}xZrx)_2O_7$ and 4 mol% $Y_2O_3$ stabilized zirconia after high temperature heat treatment. *Ceramics International*, vol. 46, no. 4, p. 4142-4147, **DOI:10.1016/j.ceramint.2019.10.130**.

[2] Góral, A., Żórawski, W., Lityńska-Dobrzyńska, L. (2014). Study of the microstructure of plasma sprayed coatings obtained from $Al_2O_3$–$13TiO_2$ nanostructured and conventional powders. *Materials Characterization*, vol. 96, p. 234-240, **DOI:10.1016/j.matchar.2014.08.016**.

[3] Pawłowski, L. (2008). *The Science and Engineering of Thermal Spray Coatings*. 2nd ed. John Wiley & Sons, Chichister.

[4] Góral, A., Lityńska-Dobrzyńska, L., Żórawski, W., Berent, K., Wojewoda-Budka, J. (2013). Microstructure of $Al_2O_3$-$13TiO_2$ coatings deposited from nanoparticles by plasma spraying. *Archives of Metallurgy and Materials*, vol. 58, no. 2, p. 335-339, **DOI:10.2478/v10172-012-0194-1**.

[5] Kusiński, J., Kac, S., Kowalski, K., Dosta, S., Georgiou, E.P., Garcia-Forgas, J., Matteazzi, P. (2018). Microstructure and properties of TiC/Ti coatings deposited by the supersonic cold gas spray technique. *Archives of Metallurgy and Materials*, vol. 63, no. 2, p. 867-873, **DOI:10.24425/122416**.

[6] Wolfe, D.E., Eden, T.J., Potter, J.K., Jaroh, A.P. (2006). Investigation and characterization of $Cr_3C_2$-based wear-resistant coatings applied by the cold spray process. *Journal of Thermal Spray Technology*, vol. 15, p. 400-412, **DOI:10.1361/105996306X124400**.

[7] Matthews, S., James, B., Hyland, M. (2009). The role of microstructure in the mechanism of high velocity erosion of $Cr_3C_2$–NiCr thermal spray coatings: Part 1 – As-sprayed coatings. *Surface and Coatings Technology*, vol. 203, no. 8, p. 1086-1093, **DOI:10.1016/j.surfcoat.2008.10.005**.

[8] Roy, M., Pauschitz, A., Bernardi, J., Koch, T., Franek, F. (2006). Microstructure and mechanical properties of

HVOF sprayed nanocrystalline $Cr_3C_2$-25(Ni20Cr) coating. *Journal of Thermal Spray Technology*, Vol. 15, p. 372-381, **DOI:10.1361/105996306X124374**.

**[9]** Fernandez, R., Jodoin, B. (2017). Effect of particle morphology on cold spray deposition of chromium carbide-nickel chromium cermet powders. *Journal of Thermal Spray Technology*, vol. 26, p. 1356-1380, **DOI:10.1007/s11666-017-0580-3**.

**[10]** Zavareh, M.A., Sarhan, A.A.D.M., Razak, B.B., Basirun, W.J. (2015). The tribological and electrochemical behaviour of HVOF-sprayed $Cr_3C_2$–NiCr ceramic coating on carbon steel. *Ceramics International*, vol. 41, no. 4, p. 5387-5396, **DOI:10.1016/j.ceramint.2014.12.102**.

**[11]** Zhang, L., Hou, J.B. (2013). Study of microstructure and phase of plasma sprayed $Cr_3C_2$-NiCr coating before and after the sparking plasma sintering. *Physics Procedia*, vol. 50, p. 293-296, **DOI:10.1016/j.phpro.2013.11.047**.

**[12]** Wolfe, D., Eden, T. (2007). Cold spray particle deposition for improved wear resistance. Champagne, V.K. (ed). *The Cold Spray Materials Deposition Process. Fundamentals and Applications*. Woodhead Publishing, Cambridge, p. 264-301, **DOI:10.1533/9781845693787.3.264**.

**[13]** Wang, Y., Normand, B., Mary, N., Yu, M., Liao, H. (2017). Effects of ceramic particle size on microstructure and the corrosion behavior of cold sprayed SiCp/Al 5056 composite coatings. *Surface and Coatings Technology*, vol. 315, p. 314-325, **DOI:10.1016/j.surfcoat.2017.02.047**.

**[14]** Silva, F.S., Cinca, N., Dosta, S., Cano, I.G., Guilemany, J.M., Benedetti, A.V. (2017). Cold gas spray coatings: basic principles, corrosion protection and applications. *Eclética Química Journal*, vol. 42, no. 1, p. 9-32, **DOI:10.26850/1678-4618eqj.v42.1.2017.p09-32**.

**[15]** Sova, A., Papyrin, A., Smurov, I. (2009). Influence of ceramic powder size on process of cermet coating formation by cold spray. *Journal of Thermal Spray Technology*, vol. 18, no. 4, p. 663-641, **DOI:10.1007/s11666-009-9359-5**.

**[16]** Champagne, V.K. (2007). Introduction, Champagne, V.K. (ed.) *The Cold Spray Materials Deposition Process. Fundamentals and Applications*. Woodhead Publishing, Cambridge, p. 1-7, **DOI:10.1533/9781845693787.1**.

**[17]** Schmidt, T., Gärtner, F., Stoltenhoff, T., Kreye, H., Assadi, H. (2005). High velocity impact phenomena and coating quality in cold spraying. *Proceedings of the International Thermal Spray Conference*, p. 232-238.

**[18]** Klassen, T., Kliemann, J.O., Onizawa, K., Donner, K., Gutzmann, H., Binder, K., Schmidt, T., Gartner, F., Kreye, H. (2009). Cold spraying – new developments and application potential. 8th Kolloquium HVOF Spraying, 9-16.

**[19]** Grujicic, M. (2007). Particle/substrate interaction in the cold-spray bonding process. Champagne, V.K. (ed). *The Cold Spray Materials Deposition Process. Fundamentals and Applications*. Woodhead Publishing Limited, Cambridge, p. 148-177, **DOI:10.1533/9781845693787.2.148**.

**[20]** ASM International Handbook Committee (2004). *Thermal Spray Technology ASM Handbook*. ASM International, Materials Park.

**[21]** Schmidt, T., Gärtner, F., Assadi, H., Kreye, H. (2006). Development of a generalized parameter window for cold spray deposition. *Acta Materialia*, vol. 54, no. 3, p. 729-742, **DOI:10.1016/j.actamat.2005.10.005**.

**[22]** Góral, A., Żórawski, W., Czaja, P., Lityńska-Dobrzyńska, L., Makrenek, M., Kowalski, S. (2019). Effect of powder morphology on the microstructure and properties of cold sprayed Ni coatings. *International Journal of Materials Research*, vol. 110, no. 1, p. 49-59, **DOI:10.3139/146.111698**.

**[23]** Sevillano, F., Poza, P., Munez, C.J., Vezzu, S., Rech, S., Trentin, A. (2012). Cold-sprayed Ni-$Al_2O_3$ coatings for applications in power generation industry. *Journal of Thermal Spray Technology,* vol. 22, no. 5, p. 772-782, **DOI:10.1007/s11666-013-9890-2**.

**[24]** Celotto, S., Pattison, J., Ho, J.S., Johnson, A.N., O'Neill, W. (2007). The economics of the cold spray process. Champagne, V.K. (ed.). *The Cold Spray Materials Deposition Process. Fundamentals and Applications*. Woodhead Publishing, Cambridge, p. 72-101, **DOI:10.1533/9781845693787.1.72**.

**[25]** Kosarev, V.F., Klinkov, S.V., Papyrin, A.N. (2007). Supersonic jet/substrate interaction in the cold spray process. Champagne, V.K. (ed.). *The Cold Spray Materials Deposition Process. Fundamentals and Applications*. Woodhead Publishing, Cambridge, p. 178-216, **DOI:10.1533/9781845693787.2.178**.

**[26]** Alidokht, S.A., Vo, P., Yue, S., Chromik, R.R. (2017). Cold spray deposition of Ni and WC-reinforced Ni matrix composite coatings. *Journal of Thermal Spray Technology*, vol. 26, p. 1908-1921, **DOI:10.1007/s11666-017-0636-4**.

**[27]** Lee, Y.T.R., Ahrafizedeh, H., Fisher, G., McDonald, A. (2017). Effect of type of reinforcing particles on the deposition efficiency and wear resistance of low-pressure cold-sprayed metal matrix composite coatings. *Surface and Coatings Technology*, vol. 324, p. 190-200, **DOI:10.1016/j.surfcoat.2017.05.057**.

**[28]** Raoelison, R.N., Verdy, Ch., Liao, H. (2017). Cold gas dynamic spray additive manufacturing today: deposit possibilities, technological solutions and viable applications. *Materials & Design*, vol. 133, p. 266-287, **DOI:10.1016/j.matdes.2017.07.067**.

**[29]** Irissou, E., Legoux, J.-G., Arsenault, B., Moreau, C. (2007). Investigation of Al-Al2O3 cold spray coating formation and properties. *Journal of Thermal Spray Technology*, vol. 16, no. 5-6, p. 661-668, **DOI:10.1007/s11666-007-9086-8**.

**[30]** EN ISO 6507-1:2018. *Metallic Materials – Vickers Hardness Test – Part 1: Test Method*. International Organization for Standardization, Geneva.

**[31]** Helfritch, D.J. (2007). Electromagnetic interference shielding by cold spray particle deposition. Champagne, V.K. (ed.). *The Cold Spray Materials Deposition Process. Fundamentals and Applications*. Woodhead Publishing, Cambridge, p. 315-326, **DOI:10.1533/9781845693787.3.315**.